Hydroclimate changes across the Amazon lowlands over the past 45,000 years

Xianfeng Wang[1,2*], R. Lawrence Edwards[3], Augusto S. Auler[4], Hai Cheng[3,5], Xinggong Kong[6], Yongjin Wang[6], Francisco da Cruz[7], Jeffrey A. Dorale[8] & Hong-Wei Chiang[1]

[1]Earth Observatory of Singapore, Nanyang Technological University, 639798 Singapore
[2]Asian School of the Environment, Nanyang Technological University, 639798 Singapore
[3]Department of Earth Sciences, University of Minnesota, Minneapolis, MN 55455, USA
[4]Instituto do Carste, Belo Horizonte, Minas Gerais, Brazil
[5]Institute of Global Environmental Change, Xi'an Jiaotong University, Xi'an 710049, China
[6]School of Geography Science, Nanjing Normal University, Nanjing 210023, China
[7]Instituto de Geociencias, Universidade de Sao Paulo, Sao Paolo, Brazil
[8]Department of Earth & Environmental Sciences, University of Iowa, Iowa City, IA 52242, USA

Reconstructing tropical hydroclimate history has been difficult, particularly in the Amazon Basin, one of Earth's major centers of deep atmospheric convection[1,2]. There has been controversy over whether the Amazon Basin was significantly drier[3,4] or remained wet[1,5] during glacial times, largely because most study sites are located on the periphery of the basin and interpretations can be complicated by sediment preservation, uncertainties in chronology, and topographical setting[6]. Here we show that rainfall in the basin responds closely to glacial boundary condition changes in temperature and atmospheric CO_2 concentration[7]. Our results are based on a decadally resolved, U-Th dated, speleothem oxygen isotopic record through much of the last ~45,000 years from Paraíso Cave in eastern Amazonia. Rainfall in this region was substantially lower during the last glacial period, about 58% of the today's during the last glacial maximum, whereas it increased up to 142% of the today's during the mid-Holocene. As compared to cave records from the western edge of the lowlands, we find that the Amazon was widely drier during the last glacial period, with much less recycling of water and likely reduced plant transpiration, although the rainforest persisted throughout this time.

Paraíso Cave (4°4'S, 55°27'W, 60 m asl) is located near the center of the eastern Amazon lowlands, densely covered by rainforest (Methods, Extended Data Fig. 1a, b). Local climate is strongly influenced by prevailing easterlies, which transport moisture year round from the tropical Atlantic to the basin (Extended Data Fig. 2a, b). The mean annual temperature at the site is about 26^{o}C, with a small seasonal fluctuation of ~2^{o}C. The annual precipitation exceeds 2,400 mm, with nearly 70% during the wet season (November to June, Extended Data Fig. 2c).

Our results are based on high-resolution speleothem oxygen isotope analysis on 7 calcite specimens, broken and columnar in shape when collected from Paraíso Cave (Methods, Extended Data Figs. 3a, b). Their chronologies were determined by a recently improved U-Th dating technique (Methods). Thanks to high U (up to 40 ppm) but low Th (as low as 10 ppt) concentrations, sample ages are well constrained. The record is made up of 106 U-Th dates, and 2,196 oxygen and carbon stable isotope analyses, and has a temporal resolution in terms of stable isotope measurements of 5 to 30 years (Fig. 1).

The Paraíso Cave record spans the last 45 thousand years (kyr), with the exception of three short gaps (Methods). Paraíso δ^{18}O shifted between -3.0 to -5.0‰ on millennial timescales during 25 - 45 kyr BP (BP: before present, present=1950 A.D.) in Marine Isotope Stage 3 (MIS 3). Subsequent to this interval, δ^{18}O increased, reaching values as high as -2.3‰ between 19 and 21 kyr BP, during the last glacial maximum (LGM). The oxygen isotopic ratio broadly decreased through the last deglaciation, reaching about -4.0‰ between 14.9 and 16.8 kyr BP (at about the time of Heinrich stadial 1 (HS1)). δ^{18}O continued to decrease and reached values of -6.0‰ in the early Holocene, and then a minimum of ~ -8.7‰ during the mid-Holocene, between 5 and 6 kyr BP, before increasing to the modern value of -6.0‰. The two most remarkable aspects of the Paraíso record are the large, dramatic shift in δ^{18}O values from the glacial period to Holocene, a shift of 6.4‰, and the millennial-scale features in the glacial period (Fig. 1).

The replicating δ^{18}O profiles of contemporaneous growth intervals of different stalagmites, together with other lines of evidence (Methods, Extended Data Fig. 4a, b; 5a, b), demonstrate that the $\delta^{18}O$ change is dominated by climate signal, rather than disturbance from water/rock interactions or kinetic fractionation. As it is unlikely that cave temperature has changed more than 5-6°C over the past 45 kyr in the tropical lowlands[8,9], we infer that most of the $\delta^{18}O$ variability in our record results from changes in precipitation $\delta^{18}O$.

The eastern Amazon underlies an enormous atmospheric deep convection zone, a landward extension of the intertropical convergence zone (ITCZ). Because of its proximity to the tropical Atlantic Ocean, moisture entering this region has undergone only minor water recycling along air transport routes[10]; changes in rainfall $\delta^{18}O$ therefore largely reflect a Rayleigh fractionation process when water vapor enriched in ^{18}O is progressively removed from air masses. Indeed, meteorological observations and model simulations show that variation of regional rainfall $\delta^{18}O$ is dominantly controlled by precipitation amount[11-13]. If so, Paraíso $\delta^{18}O$ is negatively correlated to rainfall, and is largely determined by moist convection in the eastern Amazon.

The large shift of $\delta^{18}O$ values in the Paraíso record indicates a substantial increase of convection intensity and rainfall over the eastern basin from glacial times to the Holocene. Considering that the tropical Atlantic is the single dominant moisture source, we can use the Rayleigh distillation model[11] as an approximation to calculate the fraction of water vapor lost from air masses between the tropical Atlantic and the eastern Amazon (Methods, Extended Data Fig. 1b). A similar calculation is valid for glacial times as well, because the continental shelf off the Amazon River mouth was not widely exposed even during the LGM[2]. We assume that, relative to the pre-industrial present, the Amazon Basin endured a cooling of ~ 5°C in the LGM[8], but a subtle warming of ~ 0.5°C in mid-Holocene[14] (Methods). The percentage of water vapor lost before reaching Paraíso is then about 28%, 50% and 36% during the LGM, mid-Holocene and today, respectively (Methods, Extended Data Table 1a, b). As the relative humidity likely remained close to 100% in the deep basin, then the precipitation amount integrated from source to the cave site was about 142% and 58% of the today's during the mid-Holocene and LGM, respectively.

What may have caused such large changes of precipitation in the eastern Amazon? Local summer insolation is often suggested as the major factor forcing hydroclimate change in the region[1,15-17]. The overall Paraíso record however does not obviously follow local insolation change, although it covers two precessional cycles (Fig. 1, Extended Data Fig. 6). The largest shift of Paraíso $\delta^{18}O$ occurred during the last deglaciation, the time interval that evidenced an increase of about 1/3 in atmospheric CO_2 concentration[7] (Fig. 1, Extended Data Fig. 7). Proxy data and climate model simulations have indicated a pivotal role of CO_2 in driving the deglacial warming[18]. The reduced influence of insolation in our record therefore probably implies that at least in the eastern Amazon lowlands, regional convection is largely controlled by temperature change associated with atmospheric CO_2 levels. During the LGM, a ~2-3^{o}C drop in sea surface temperature (SST) in the equatorial western Atlantic[19] accompanied by a cooling of ~5^{o}C on land[8] could suppress moisture supply from the ocean and reduce convection in the basin[20]. In contrast, warming in mid-Holocene likely enhanced the upward motion of moisture and resulted in more abundant precipitation. The ~2.3‰ $\delta^{18}O$ increase through the last 5,000 years however may not solely be attributed to a temperature change which was rather subtle[14]. Under modern climatic conditions, periodic Amazon droughts, in particular in the eastern and central regions, are closely tied to positive SST anomalies in the eastern tropical Pacific[21]. Thus, a strengthening of El Niño/Southern Oscillation (ENSO) activity[22] could exacerbate rainfall decrease and water $\delta^{18}O$ increase after the mid-Holocene. Alternatively, under interglacial boundary conditions, it is possible that local insolation[1, 15-17] contributed to the observed Holocene changes.

During MIS 3, the Paraíso record shows strong millennial-scale variability, as a manifestation of Heinrich and Dansgaard-Oeschger (D/O) events. These variations coincide with, but in an anti-phased fashion, their counterparts observed in eastern China[23,24] and can also be correlated one-to-one to the rapid events in Greenland and Antarctica[25] (Fig. 2, Extended Data Fig. 8a, b). The latitudinal displacement of the mean position of the ITCZ, in response to changes in the Atlantic meridional ocean circulation (AMOC), may well cause the anti-phased abrupt change in rainfall between the two lowlatitudes[15]. Perturbations in the AMOC can induce SST anomalies in the tropical oceans, which then alter moist convections and rainfall in the region. In this regard, the remarkably tight correlations among these records reinforce the notion that abrupt changes occurring in the high-latitudes can be rapidly propagated in the climate system, likely through an atmospheric linkage[15].

Were the aforementioned large glacial to Holocene rainfall changes mainly confined to the eastern Amazon or more extensive in the lowlands? Existing records from the Amazon Basin and its surrounding areas draw a contentious picture of rainfall changes during the LGM and the last deglaciation, compromised by less than ideal chronological control, sediment preservation and topographic effects (e.g., refs. 1-6). Meanwhile, several studies suggest a strong South American Summer Monsoon (SASM) intensity during the LGM and hence higher rainfall in the central Andes and southern Brazil[1,15,16]. But, these sites are not located within the basin itself.

We here compare the Paraíso record with speleothem $\delta^{18}O$ profiles obtained from caves in the western lowlands near the eastern flank of the Andes (5°44'S, 77°30'W, ~960 m asl.; Extended Data Figs. 1a, b)[9,17] to assess surface moisture transport across the basin and spatial changes in precipitation (Fig. 3). A significant $\delta^{18}O$ offset, ~ 4.5‰ – 5.1‰ exists during MIS 3, between the Paraíso record from eastern Amazon and the temperature-effect corrected Diamante-Tigre Perdido record from western Amazon (Methods). Whereas the oxygen isotope ratio in Paraíso samples is higher, varying between -3.0‰ to -5.0‰, $\delta^{18}O$ values are about -8.1 to -9.5‰ in the Diamante profile after correction for isotopic fractionation caused by cave temperature differences. This east to west difference is further enhanced during the LGM, by up to 6.6‰. However, the two records show similar values during the early-mid Holocene and their values differ by only ~2.5‰ at present.

The change of $\delta^{18}O$ offset between the two records, which essentially describes a change in the gradient of rainfall $\delta^{18}O$ across the basin, signifies a shift of dominant isotope fractionation process over time. Lower $\delta^{18}O$ values in the western Amazon samples relative to those in Paraíso are consistent with the overall continental rainout effect of water isotopes[11] when surface moisture is transported from the east to the west across the lowlands. Indeed, given the vast distance between the two locations (~2,400 km), the spatial rate of speleothem $\delta^{18}O$ change is -1.0‰/1,000 km, in concert with the precipitation $\delta^{18}O$ gradient observed today in the lowland, -0.1‰ per degree longitude[12]. This gradient is however very low, largely due to water recycling in the basin, through plant transpiration in particular. Plant transpiration supplies moisture downwind, yet does not induce water isotope fractionation when the ambient humidity is high in the tropics[26,27]. Such an effect, probably due to the much denser rainforest coverage in the basin, almost completely dominates during the early-mid Holocene, as shown in the nearly identical $\delta^{18}O$ values of the two speleothem records. In contrast, the precipitation $\delta^{18}O$ gradient reached as high as -2.8‰/1,000 km during the LGM. This strongly suggests that during glacial time, the Amazon Basin was significantly drier with reduced rainforest coverage, in accordance with the studies on marine and lacustrine sediments[2,4]. Therefore, the continental effect dictated the isotopic fractionation and led to a progressive depletion of ^{18}O in rainfall when moisture was transported across the basin, whereas the effect of plant transpiration was much less.

As the largest tropical wetland, a dry Amazon Basin during the LGM probably contributed to the drop of atmospheric CH_4 recorded in ice cores (Extended Data Fig. 7). This may explain the controversy that Asian monsoon intensity was relatively strong during the LGM, while atmospheric CH_4 abundance declined to the lowest[7,23]. During MIS 3, a positive correlation however exists between the CH_4 concentration and Paraíso $\delta^{18}O$ on the millennial timescale, which confirms that Northern Hemisphere tropical and boreal wetlands have been the dominant sources of methane[7,24]. In contrast to a dry Amazon, the values of $\delta^{13}C$ in Paraíso stalagmites can be as low as -10‰ during the LGM, comparable with those in Holocene samples (Extended Data Fig. 9). This indicates that the Amazon Basin was not dry enough during the LGM or any time within the last 45 kyr for the forest to have turned into a savanna with significant C4 vegetation. Rainforest has persisted in the eastern Amazon even when rainfall amounts were only about 60% of today's values during the LGM.

If our observed pattern of Amazonian hydroclimate change from the last glacial period to Holocene can be extrapolated to a CO_2-induced warming future, rainfall in the Amazon lowlands would be expected to increase substantially, being consistent with the "wet wetter, dry drier" mechanism[28]. Ironically, ongoing deforestation and expansion of plantations in the basin, particularly in the eastern region, as well as a possible intensification of ENSO[21,29], may however reduce water recycling through plant transpiration; therefore, this would reduce moisture delivery to the west[30]. Whether or not the long-lasting Amazon rainforest can be sustained in the future remains an open question.

References:

1. Baker, P. A. *et al.* The history of South American tropical precipitation for the past 25,000 years. *Science* **291**, 640-643 (2001).
2. Maslin, M. A. *et al.* Dynamic boundary-monsoon intensity hypothesis: evidence from the deglacial Amazon River discharge record. *Quat. Sci. Rev.* **30**, 3823-3833 (2011).
3. Ledru, M.-P., Bertaux, J. & Sifeddine, A. Absence of Last Glacial Maximum records in lowland tropical forests. *Quat. Res.* **49**, 233-237 (1998).
4. D'Apolito, C., Absy, M. L. & Latrubesse, E. M. The Hill of Six Lakes revisited: new data and re-evaluation of a key Pleistocene Amazon site. *Quat. Sci. Rev.* **76**, 140-155 (2013).
5. Colinvaux, P. A. *et al.* A long pollen record from lowland Amazonia: Forest and cooling in glacial times. *Science* **274**, 85-88 (1996).
6. Baker, P. A. & Fritz S. C. Nature and causes of Quaternary climate variation of tropical South America. *Quat. Sci. Rev.* **124**, 31-47 (2015).
7. Marcott, S. A. *et al.* Centennial-scale changes in the global carbon cycle during the last deglaciation. *Nature* **514**, 616-619 (2014).
8. Stute, M. *et al.* Cooling of tropical Brazil (5^{o}C) during the Last Glacial Maximum. *Science* **269**, 379-383 (1995).
9. van Breukelen, M. R. *et al.* Fossil dripwater in stalagmites reveals Holocene temperature and rainfall variation in Amazonia. *Earth Planet. Sci. Lett.* **275**, 54-60 (2008).
10. Eltahir, E. A. B. & Bras, R. L. Precipitation recycling in the Amazon Basin. *Q. J. R. Meteorol. Soc.* **120**, 861-880 (1994).
11. Dansgaard, W. Stable isotopes in precipitation. *Tellus* **16**, 436-486 (1964).
12. Vuille, M. *et al.* Modeling δ^{18}O in precipitation over the tropical Americas: 1. Interannual variability and climatic controls. *J. Geophys. Res.* **108**, D6, 4174, doi:10.1029/2001JD002038 (2003).
13. Lee, J.-E., Johnson, K. & Fung, I. Precipitation over South America during the Last Glacial Maximum: An analysis of the "amount effect" with a water isotope-enabled general circulation model. *Geophys. Res. Lett.* 36, L19701, doi:10.1029/2009GL039265 (2009).

14. Wanner, H. *et al.* Mid- to late Holocene climate change: an overview. *Quat. Sci. Rev.***27**, 1791-1828 (2008).
15. Wang, X. *et al.* Millennial-scale precipitation changes in southern Brazil over the past 90,000 years. *Geophys. Res. Lett.* 34, L23701, doi:10.1029/2007GL031149 (2007).
16. Cruz, F. W. *et al.* Orbitally driven east-west antiphasing of South American precipitation. *Nature Geosci.* **2**, 210-214 (2009).
17. Cheng, H., *et al.* Climate change patterns in Amazonia and biodiversity. *Nature Comm.* **4,** 1411 (2013).
18. Shakun, J. D. *et al.* Global warming preceded by increasing carbon dioxide concentrations during the last deglaciation. *Nature* **484**, 49-54 (2012).
19. Jaeschke, A., Rühlemann, C., Arz, H., Heil, G. & Lohmann, G. Coupling of millennial-scale changes in sea surface temperature and precipitation off northeastern Brazil with high-latitude climate shifts during the last glacial period. *Paleoceanography* **22**, PA4206, doi:10.1029/2006PA001391 (2007).
20. Cook, K. H. & Vizy, E. K. South American climate during the Last Glacial Maximum: Delayed onset of the South American monson. *J. Geophys. Res.* **111**, D02110 doi:10.1029/2005JD005980 (2006).
21. Malhi, Y. *et al.* Climate change, deforestation, and the fate of the Amazon. *Science* **319**, 169-172 (2008).
22. Koutavas, A. & Joanides, St. El Niño-Southern Oscillation extrema in the Holocene and Last Glacial Maximum. *Paleoceanography* **27**, PA4208, doi:10.1029/2012PA002378 (2012).
23. Wang, Y. J. *et al.* A high-resolution absolute-dated Late Pleistocene monsoon record from Hulu Cave, China. *Science* **294**, 2345–2348 (2001).
24. Cheng, H. *et al.* The Asian monsoon over the past 640,000 years and ice age terminations. *Nature* **534**, 640-646 (2016).
25. WAIS Divide Project Members. Precise interpolar phasing of abrupt climate change during the last ice age. *Nature* **520**, 661-665 (2015).
26. Salati, E., Dall'Olio, A., Matsui, E. & Gat, J. R. Recycling of water in the Amazon Basin: An isotopic study. *Water Resour. Res.* **15**, 1250-1258 (1979).

27. Winnick, M. J., Chamberlain, C. P., Caves, J. K. & Welker, J. M. Quantifying the isotopic ‘continental effect’. *Earth Planet. Sci. Lett.* **406**, 123-133 (2014).
28. Held I. M. & Soden, B. J. Robust response of the hydrological cycle to global warming. *J. Climate* **19**, 5686-5699 (2006).
29. Vecchi, G. A. *et al.* Weakening of tropical Pacific atmospheric circulation due to anthropogenic forcing. *Nature* **441**, 73-76 (2006).
30. Spracklen, D. V., Arnold, S. R. & Taylor, C. M. Observations of increased tropical rainfall preceded by air passes over forests. *Nature* **489**, 282-285 (2012).

Online Content Methods, along with any additional Extended Data display items and Source Data, are available in the online version of the paper; references unique to these sections appear only in the online paper.

Acknowledgements This work was supported by a Singapore NRF Fellowship NRFF2011-08 and a Gary Comer Fellowship to X.W., US NSF grants 1103404 and 1317693 to R.L.E. and H.C., Brazil CNPq grant 540064/01-7 to A.S.A, China NBRP 2013CB955902, NSFC 41230524 to H.C. Field traveling funds were partially supported by a National Geographical Society grant 7574-03. We acknowledge the help of colleagues of Grupo Bambuí de Pesquisas Espeleológicas with cave mapping and sampling. We thank R. Richardo, S. Yuan, Y. Lu and Y. Djamil for their assistances with the figures on wind fields and regional rainfall, and thank B. Wohlfarth and S. Hemming for the discussions during the manuscript preparation.

Author Contributions X.W., R.L.E., and A.S.A. designed the project. X.W., A.S.A., and J.A.D. performed the fieldwork and sampling. X.W. and H.-W. C. did the U-Th dating. X.W., X.K., and Y.W. contributed to the oxygen isotope measurements. X.W. wrote the manuscript, which was edited by R.L.E. and other co-authors. All authors discussed the results and implications and commented on the manuscript at all stages.

Author Information The authors declare no competing financial interests. Correspondence and requests for materials should be addressed to X.W. (xianfeng.wang@ntu.edu.sg).

Figure 1 | Paraíso speleothem record and its comparisons with local summer insolation, tropical Atlantic SST and atmospheric CO_2 concentration. a, The Paraíso record is spliced by replicated $\delta^{18}O$ profiles from 7 stalagmite samples. U-Th dates and error bars (2σ) are color coded with samples. It covers the past 45,000 years, with three short gaps, ~16.6-18.0 kyr BP, ~10.9-15.0 kyr BP, and ~6.3-7.6 kyr BP, respectively. **b,** 5°S January insolation (in gray). Note the insolation is plotted in a reversed scale as proposed in ref. 16. The correlation between the Paraiso $\delta^{18}O$ and local insolation is however not strong. See Extended Data Fig. 6 for more details. **c,** Tropical Atlantic alkenone SST reconstruction from sediment core GeoB 3910-2 (in dark blue, ref. 19). **d,** Atmospheric CO_2 concentration change[7] (in blue, also see Extended Data Fig. 7). ppmv, parts per million by volume.

Figure 2 | Comparisons of the eastern Amazon and eastern China stalagmite records. a, An opposite correlation can be observed between the eastern Amazon (Paraíso, in red and pink) and eastern China (Hulu, in blue)[24] stalagmite $\delta^{18}O$ records on the millennial timescales during the time interval from 25 kyr BP to 45 kyr BP, suggesting an anti-phased relationship on rainfall between the two regions. The D/O events are also marked. **b,** The strong anti-phased correlation between the two records on millennial timescales can be confirmed by squared wavelet coherence (http://noc.ac.uk/using-science/crosswavelet-wavelet-coherence) of the two standardized time series. The 5% significance level against red noise is shown as a thick contour. The relative phase relationship between the two time series is shown as arrows, with anti-phase pointing left.

Figure 3 | Comparisons of the eastern and western Amazon speleothem records. The eastern Amazon $\delta^{18}O$ record (red) is from Paraíso cave, and the speleothem $\delta^{18}O$ records in the western Amazon are from Diamante[17] (blue) and Tigre Perdido[9] (dark blue) caves All three records are absolutely dated with U-Th dating techniques. The original records from western Amazon are shown in gray. They were then shifted 1.4‰ negatively to account for the oxygen isotopic fractionation due to cave temperature difference between the western sites and Paraíso cave in the east (Methods).

METHODS

Cave location and samples Paraíso Cave (04°04'S, 55°27'W, 60 m asl) is located near the center of the eastern Amazon lowlands, adjacent to the Tapajós River, which is one of the main tributaries of the Amazon River (Extended Data Fig. 1a, b). The cave is ~1.6 km long, overlaid by ~15 m-thick Pennsylvanian limestone of Itaituba Formation and covered by dense tropical rainforest. The cave has a small single entrance. Gravels and boulders nearly block the initial chamber that declines gradually toward an underground stream. The cave therefore has a very high relative humidity, near 100%.

We collected mostly broken columnar stalagmites due to easiness of sampling and conservation reasons. They were collected from scattered locations inside the cave. The stalagmites were cut into halves along their growth axes and their surfaces were polished. Seven of them were selected for this study. They are all comprised of calcite, and some have clear banding structures.

Analytical methods A total of 106 subsamples (16, 8, 13, 12, 41, 3 and 13 for stalagmites PAR01, PAR03, PAR16, PAR06, PAR07, PAR08 and PAR24, respectively) were drilled for U-Th dating. Procedures for chemical separation and purification of uranium and thorium are similar to those described in refs. 31, 32. The dating analysis was performed at the Minnesota Isotope Laboratory, University of Minnesota, on a ThermoFinnigan Neptune multi-collector inductively coupled plasma mass spectrometer (MC-ICP-MS), and also on a Neptune Plus instrument housed in a newly established isotope geochemistry laboratory at the Earth Observatory of Singapore, Nanyang Technological University. The measurements largely followed the methods described in refs. 33, 34. All the U and Th isotopes, except ^{238}U and ^{232}Th, were measured with a peak-jumping mode on a secondary electron multiplier (SEM) equipped with a retardation potential quadrupole lens (RPQ) to improve abundance sensitivity. Consistent results were achieved on solution aliquots between the two labs.

All the stalagmite samples have high U concentration (a few parts per million, ppm) but very low Th concentration (typically in n x 10 or n x 100 parts per trillion, ppt) (Extended

Data Fig. 3). The measured $^{230}Th/^{232}Th$ is in a range of n x 1,000 to n x 1,000,000 ppm in atomic ratio. We calculated corrected ^{230}Th ages using the bulk Earth initial $^{230}Th/^{232}Th$ value of 4.4 ppm in atomic ratio, with an arbitrary uncertainty of 50%. Whatever the true initial $^{230}Th/^{232}Th$ value is, its contribution to the final U-Th ages should be negligible. Uncertainties in the U-Th isotopic data and ^{230}Th dates are then calculated at 2σ level or two standard deviations of the mean. The typical relative error in age is less than 0.5%.

The U-Th ages for all the stalagmite samples are in stratigraphic order. The stalagmites have relatively fast and constant growth rates (Extended Data Fig. 3a, b). Their age models were hence established by linear interpolations.

Oxygen and carbon stable isotope analyses of stalagmite samples were done in the School of Geography Science, Nanjing Normal University, China. Calcite powder subsamples were milled with dental drill bits at 1-5 mm intervals and analyzed on a Finnigan MAT 253 mass spectrometer equipped with a Kiel Carbonate Device III. Duplicate measurements of standard NBS19 and arbitrary samples show a long-term reproducibility of ~0.10‰ (1σ). In total, 2,196 O and C isotopic measurements were performed, including 449, 145, 406, 110, 820, 100 and 166 analyses from stalagmites PAR01, PAR03, PAR16, PAR06, PAR07, PAR08 and PAR24, respectively. This yields a temporal resolution about 5 to 30 years, slightly higher in the Holocene part than that during the last glacial period portion. Stable isotopic results are reported in per mil (‰), relative to the Vienna Pee Dee Belemnite (VPDB) standard ($\delta^{18}O = [((^{18}O/^{16}O)_{sample} / (^{18}O/^{16}O)_{VPDB}) - 1] \times 1{,}000$‰).

Speleothems often have growth discontinuities due to a wide range of factors, including changes of sea level, soil temperature, regional aridity, local cave flooding or drip water dynamics[35]. Among the seven calcite specimens we used to construct the Paraíso Cave record, samples PAR06, PAR07, PAR16 and PAR24 present detectable growth hiatuses (Extended Data Fig. 3b). Nevertheless, the striking similarities between their $\delta^{18}O$ profiles over the contemporaneous growth periods of the seven samples, strongly argue for the dataset robustness. We hereby obtained a spliced record which spans the past

45,000 years, with three short gaps, ~16.6-18.0 kyr BP, ~10.9-15.0 kyr BP, and ~6.3-7.6 kyr BP, respectively.

Equilibrium condition tests on carbonate deposition Many processes other than climate, such as water-rock interactions in vadose zone and kinetic fractionation during carbonate precipitation, could contribute to stable isotopic signal in speleothems. It is however very unlikely that the combination of hydrological processes experienced by water drips are identical, especially if we consider different growth rate in samples and carbonate super-saturation state in water films[23,36].

Paraíso $\delta^{18}O$ profiles present substantial replications between different samples even when their growth rates are different by a factor of 10 (e.g., between PAR07 and PAR08, Extended Data Figure 3b). Although no contemporaneous samples have been found yet during the LGM, PAR07 and PAR24 cover 19.0 to 20.7 kyr BP and 21.0 to 22.8 kyr BP, respectively. Their $\delta^{18}O$ values during the LGM are essentially the same, -2.72‰ ± 0.23‰ (1σ) and -2.79‰ ± 0.19‰ (1σ), respectively. Therefore, the replication between the $\delta^{18}O$ profiles of contemporaneous samples strongly advocates that Paraíso Cave speleothems were mostly deposited under equilibrium conditions and that the influence of kinetic fractionation on the $\delta^{18}O$ record must be negligible.

The low correlation coefficients between the $\delta^{18}O$ and $\delta^{13}C$ in most Paraíso Cave samples (Extended Data Fig. 4a, b), in addition, confirm that kinetic CO_2 degassing and water evaporation should have been minimal during calcite precipitation[37]. We further tested the equilibrium conditions in Paraíso Cave modern calcite depositions. The $\delta^{18}O$ values of ~ -5.7‰ in modern calcite are in a good approximation to the predict value of ~ -5.8‰ under equilibrium conditions with a cave temperature of 26°C and annual average rainfall $\delta^{18}O$ of ~ -4.2‰ (refs. 38, 39). All these lines of evidence suggest that calcite precipitation in Paraíso Cave mostly takes place under equilibrium conditions. Therefore, $\delta^{18}O$ signal in Paraíso Cave speleothems is dominated by climate variation at the time of calcite precipitation.

Calculations on moisture rainout in eastern Amazon Paraíso Cave is in relative proximity to the coast. Moisture is brought into the region by the prevailing easterlies and has not endured strong water recycling along the air trajectory[10,40]. When water vapor is progressively removed from air masses during the transport, the Rayleigh fractionation dictates and results in a gradual depletion of ^{18}O in the remaining water vapor and subsequent precipitation[11]. We therefore, to first order, can use the standard Rayleigh distillation model to calculate to what fraction moisture has been removed when it is integrated from the source region to the cave site (Extended Data Table 1). For the calculation, we here adopt the equation: $(1000 + \delta^{18}O_p) / (1000 + \delta^{18}O_{sw}) = f^{(\alpha - 1)}$, where $\delta^{18}O_p$ and $\delta^{18}O_{sw}$ are $\delta^{18}O$ of meteoric precipitation and seawater, respectively, f is the fraction of the original water vapor remaining in air masses, and α is the water/vapor fractionation factor.

The same calculation can be applied to moisture transport in the past, such as during the mid-Holocene and the LGM, because the exposure and submergence of the narrow continental shelf did not change dramatically the distance between the cave site and moisture source[2]. Here the time intervals of modern, mid-Holocene, and the LGM cover the last 1,000 years or so, the period about 5,000-6,000 years BP, and the period about 19,000 to 23,000 years BP, respectively, as defined in refs 14, 41, and 42.

Relative to today's temperature of 26 ^{o}C, we assign 26.5 ^{o}C and 21 ^{o}C to the cave temperature during the mid-Holocene and LGM, respectively (Extended Data Table 1a). This is after taking into consideration of SST change in the tropical Atlantic[14,19,42,43], as well as surface temperature change reported from higher altitudes or further inland in few early studies[5,8,9]. The uncertainty of temperature estimation at the cave site is probably within 1^{o}C. To test the sensitivity of water vapor loss to temperature, we also applied different temperatures for the mid-Holocene (e.g., the same as modern) and LGM (e.g., 4^{o}C or 6^{o}C lower than today's value) (Extended Data Table 1b). The calculations show that the bulk estimations of water vapor loss are not sensitive to temperature change within the uncertainties of paleo-temperature reconstructions[5,8,14].

In the equatorial lowlands, it is reasonable to assume that the relative humidity is close to 100%, even when the surface temperature was ~5 ^{o}C lower during the LGM. We can thus further evaluate the absolute amount of moisture change through time (Extended Data Table 1a, b).

The decrease in temperature and precipitation during the LGM could affect water balance in the region. At present, mean annual rainfall is ~2,400 mm in the region, substantially higher than the annual evapotranspiration of ~1,200 mm (Extended Data Fig. 5a). If we assume that rainfall seasonality remained similar during the LGM in the wet tropics, water balance estimation[44,45] shows that through most of the months, precipitation could have remained higher than actual evapotranspiration (Extended Data Fig. 5b). Therefore, seasonal groundwater recharge did not change much during the LGM to cause biases in the stable isotopic composition of Paraíso cave drip water.

Calculations on the east-west Amazon moisture isotope gradient We can study changes of the moisture isotope gradient across the Amazon lowland by comparing cave $\delta^{18}O$ records from nearly the two longitudinal ends of the basin. For this study, we chose the speleothem records from Diamante Cave[17] and Cueva del Tigre Perdido[9], both located in the western lowland (5°44'S, 77°30'W, ~960 m asl) and compared them with the Paraíso record from the east. The Diamante record extends continuously through the discussed time period, and its U-Th dates are better constrained relative to other cave records in the region. Cueva del Tigre Perdido is located near Diamante Cave, and shares the same elevation. It has higher resolution during late Holocene, so that this portion of the record was used for the spliced western profile.

In the tropics, below the height of cloud base at 950 mb, air temperature drops with an increase in altitude at a dry adiabatic lapse rate of -9.7^{o}C/km (ref. 46). Above cloud base, air temperature falls much slower, at a moist adiabatic lapse rate of -5 ^{o}C/km or less[47]. Nevertheless, because of their relatively low elevations, uncertainty in the mountain lapse rate estimation probably does not have dramatic influence on cave temperature in western

Amazon, even between the glacial and interglacial periods[48]. However, the lapse rate can cause cave temperature difference between the east and west cave sites. Due to the temperature dependent calcite-water isotopic fractionation, this contributes to the difference between calcite $\delta^{18}O$ values in the two records. We here assign a constant, typical lapse rate of 6.5 ^{o}C/km, which leads to ~5.8 ^{o}C lower in temperature (6.5 ^{o}C/km * 900 m) at Diamante-Tigre Perdido caves relative to Paraíso Cave. This number is consistent with the modern temperature difference between the caves (~26^{o}C and ~20^{o}C in Paraíso Cave and Cueva del Tigre Perdido, respectively)[9]. The temperature difference can transfer to an imprint of ~1.4‰ calcite $\delta^{18}O$ increase (-5.8 ^{o}C * (-0.24 ‰/^{o}C)) in the Diamante-Tigre Perdido record. Such temperature effect caused by elevation difference must be removed from the Diamante-Tigre Perdido record to facilitate the record comparison. We therefore shifted the western profile ~1.4‰ more negatively relative to the original record (Fig. 3). In other words, the local rainfall $\delta^{18}O$ at the Amazon western site should be lowered by ~1.4‰, assuming that carbonate deposition is under equilibrium conditions.

We calculated the offset between the two cave records by subtracting their contemporaneous $\delta^{18}O$ values. If speleothem calcite is deposited under equilibrium conditions, such offset is a good approximation to the discrepancy of rainfall $\delta^{18}O$ between the east and west cave sites after we remove the aforementioned temperature effect caused by their elevation difference. We can then obtain the precipitation $\delta^{18}O$ gradient across the Amazon Basin by dividing the offset of speleothem $\delta^{18}O$ by the longitudinal distance (~2,400 km). Changes in cave temperature and ocean reservoir $\delta^{18}O$ related to sea level fluctuations can contribute to each speleothem $\delta^{18}O$ signal, particularly on the glacial-interglacial timescales. Such effects however are in the same magnitude in the two records, and therefore should be cancelled out in the offset. Indeed, through this method, we estimated a modern spatial rate of speleothem $\delta^{18}O$ change of ~1.0‰/1,000km (~2.5‰ $\delta^{18}O$ offset divided by a distance of ~2,400 km). This is in agreement with the precipitation $\delta^{18}O$ gradient in the wetland observed today (~0.1‰ per unit longitude)[12]. We hereby believe that in the western Amazon, plant transpiration effect[26,27,49] is probably more important than rainfall amount effect in determining rainfall $\delta^{18}O$ and subsequent cave carbonate $\delta^{18}O$ values, broadly in line with the conclusions reached in ref. 17.

References:

31. Edwards, R. L., Chen, J. H. & Wasserburg, G. J. ^{238}U-^{234}U-^{230}Th-^{232}Th systematics and the precise measurement of time over the past 500,000 years. *Earth Planet. Sci. Lett.* **81**, 175–192 (1986).
32. Cheng, H. *et al.* The half-lives of uranium-234 and thorium-230. *Chemical Geology* **169**, 17-33 (2000).
33. Shen, C.-C., *et al.* High-precision and high-resolution carbonate ^{230}Th dating by MC-ICP-MS with SEM protocols. *Geochim. Cosmochim. Acta* **99**, 71-86 (2012).
34. Cheng, H. *et al*. Improvements in ^{230}Th dating, ^{230}Th and ^{234}U half-life values, and U-Th isotopic measurements by multi-collector inductively coupled plasma mass spectrometry. *Earth Planet. Sci. Lett.* **371/372**, 82-91 (2013).
35. Fairchild, I. J. & Baker, A. Speleothem science: From process to past environments. Wiley-Blackwell, Pp. 450 (2012).
36. Dorale, J. A., Edwards, R. L., Ito, E. & González, L. A. Climate and vegetation history of the mid-continent from 75 to 25 ka: a speleothem record from Crevice Cave, Missouri, USA. *Science* **282**, 1871–1874 (1998).
37. Hendy, C. H. The isotopic geochemistry of speleothems—I. The calculation of the effects of different modes of formation on the isotopic composition of speleothems and their applicability as palaeoclimatic indicators. *Geochim. Cosmochim. Acta* **35**, 801–824 (1971).
38. Bowen, G. J. Isoscapes: Spatial pattern in isotopic biogeochemistry. *Annu. Rev. Earth Planet. Sci.* **38**, 161-187 (2010).
39. Johnston, V. E., Borsato, A., Spotl, C., Frisia, S. & Miorandi, R. Stable isotopes in caves over altitudinal gradients: fractionation behavior and inferences for speleothem sensitivity to climate change. *Clim. Past* **9**, 99-118 (2013).
40. Vuille, M. & Werner, M. Stable isotopes in precipitation recording South American summer monsoon and ENSO variability: observations and model results. *Clim. Dy.* **25**, 401-413 (2005).
41. IPCC. Climate Change 2013: The Physical Science Basis. Contribution of Working Group I to the Fifth Assessment Report of the Intergovernmental Panel

on Climate Change [Stocker, T.F. *et al.* (eds.)]. Cambridge University Press, Cambridge, United Kingdom and New York, NY, USA, 1535 pp (2013).

42. MARGO Project Members. Constraints on the magnitude and patterns of ocean cooling at the Last Glacial Maximum. *Nature Geosci.* **2**, 127-132 (2009).
43. Marcott, S. A. *et al.* A reconstruction of regional and global temperature for the past 11,300 years. *Science* **339**, 1198-1201 (2013).
44. Thornthwaite, C. W. An approach toward a rational classification of climate. *Geograph. Rev.* **38**, 55–94 (1948).
45. McCabe, G. J. & Markstrom, S. L. A monthly water balance model driven by a graphical user interface. *U.S. Geological Survey Open-File report 2007-1088* (2007).
46. Betts, A. K. & Ridgway, W. Tropical boundary layer equilibrium in the last ice age. *J. Geophys. Res.* **97**, 2529-2534 (1992).
47. Kageyama, M., Harrison, S. P. & Abe-Ouchi, A. The depression of tropical snowlines at the last glacial maximum: What can we learn from climate model experiments? *Quatern. Int.* **138-139**, 202-219 (2005).
48. Broecker, W. S. Mountain glaciers: Records of atmospheric water vapor content? *Global Biogeochem. Cycles* **11**, 589-597 (1997).
49. Rozanski, K., Araguás-Araguás, L. & Gonfiantini, R. Isotopic patterns in modern global precipitation. In: Climate change in continental isotopic records [Swart, P. K., Lohmann, K. C., McKenzie, J. & Savin, S. (eds.)]. *Geophys. monogr. Ser.* **78**, 1-36 (1993).
50. Laskar, J. *et al.* A long-term numerical solution for the insolation. *Astron. Astrophys.* **428**, 261-285 (2004)
51. Luthi, D. *et al.* High-resolution carbon dioxide concentration record 650,000-800,000 years before present. *Nature* **453**, 379-382 (2008).
52. Loulergue, L. *et al.* Orbital and millennial-scale features of atmospheric CH4 over the past 800,000 years. *Nature* **453**, 383-386 (2008).
53. NGRIP Project Members. High-resolution record of Northern Hemisphere climate extending into the last interglacial period. *Nature* **431**, 147–151 (2004).

54. EPICA Community Members. One-to-one coupling of glacial climate variability in Greenland and Antarctica. *Nature* **444**, 195–198 (2006).

55. Veres, D. *et al.* The Antarctic ice core chronology (AICC2012): an optimized multi-parameter and multi-site dating approach for the last 120 thousand years. *Clim. Past* **9**, 1733–1748 (2013).

56. Svensson, A. *et al.* A 60,000 year Greenland stratigraphic ice core chronology. *Clim. Past* **4**, 47-57 (2008).

57. Wang, X. *et al.* Wet periods in northeastern Brazil over the past 210 kyr linked to distant climate anomalies. *Nature* **432**, 740-743 (2004).

58. Anderson, R. F. *et al.* Wind-driven upwelling in the Southern Ocean and the deglacial rise in atmospheric CO2. *Science* **323**, 1443-1448 (2009).

59. Broecker, W. S. Paleocean circulation during the last deglaciation: a bipolar seesaw? *Paleoceanography* **13**, 119–121 (1998).

60. Buizert, C. *et al.* The WAIS Divide deep ice core WD2014 chronology. Part 1. Methane synchronization (68–31ka BP) and the gas age–ice age difference. *Clim. Past.* **11**, 153–173 (2015).

61. Genty, D. *et al.* Precise dating of Dansgaard-Oeschger climate oscillations in western Europe from stalagmite data. *Nature* **421**, 833-837 (2003).

62. Schrag, D. P., Hampt, G. & Murray, D. W. Pore fluid constraints on the temperature and oxygen isotopic composition of the glacial ocean. *Science* **272**, 1930-1932 (1996).

63. Schrag, D. P. *et al.* The oxygen isotopic composition of seawater during the Last Glacial Maximum. *Quat. Sci. Rev.* **21**, 331-342 (2002).

64. Horita, J. & Wesolowski, D. J. Liquid-vapor fractionation of oxygen and hydrogen isotopes of water from the freezing to the critical temperature. *Geochim. Cosmochim. Acta* **58**, 3425-3437 (1994).

Extended Data Figure 1 | Cave locations and moisture pathways. a, The locations of Paraíso Cave in eastern Amazon (red rectangle), and Diamante cave[17] (blue rectangle) and Tigre Perdido cave[9] (purple rectangle) in western Amazon. Paraíso Cave is located between Belém and Manaus, adjacent to the Tapajós River. Also shown are easterlies, which carry moisture to the lowlands from the tropical Atlantic. The Amazon Basin and Andes are shown in green and brown, respectively. **b,** 72-hour back-trajectories arriving at Paraíso and western Amazonian cave sites (white stars) during wet season (in red) and dry season (in blue) averaged over 1981-2010. The background topographical map is created with grid files from the Global Multi-Resolution Topography (GMRT) Synthesis (http://www.marine-geo.org/tools/GMRTMapTool). Moisture trajectories are derived by the NOAA Hysplit model (http://ready.arl.noaa.gov/HYSPLIT.php). The moisture at Paraíso Cave site is dominantly from the tropical Atlantic, whereas precipitation received in the western Amazon has largely endured recycling in the lowlands.

Extended Data Figure 2 | Climatology of tropical South America. a, Horizontal wind over South America at 850h Pa (Vectors, m/s) from NCEP CFSR (1981-2010, http://cfs.ncep.noaa.gov/cfsr/atlas/) and precipitation (Shading, mm/day) from TRMM 3B43 (1998-2010, http://trmm.gsfc.nasa.gov/3b43.html) averaged over DJFM. **b,** As in **a**, but for JJAS. **c,** Monthly averaged temperature, precipitation and rainfall $\delta^{18}O$ over Belém (blue dots) and Manaus (green triangles). The local climate at Paraíso Cave shares the same characteristics as those of Belém and Manaus. Data are from the IAEA GNIP database (http://www-naweb.iaea.org/napc/ih/IHS_resources_gnip.html).

Extended Data Figure 3 | Paraíso calcite stalagmite and age models. a, Image of a Paraíso sample. Paraíso calcite stalagmites typically have high U concentration (up to 40 ppm) but low Th concentration (< 1 ppb), almost ideal for U-Th age determination. **b,** Age models are shown for samples PAR01, PAR03, PAR06, PAR07, PAR08, PAR16 and PAR24. The chronology of the samples is established by linear interpolation between successive U-Th dates. Dates are shown in black dots. Age uncertainties (2σ) are also presented. Most of the error bars are however smaller than the symbol size.

Extended Data Figure 4 | Scatter plots of oxygen and carbon isotope ratios. a, Relationship between $\delta^{18}O$ and $\delta^{13}C$ data of Holocene Paraíso stalagmites. **b,** As in **a**, but for glacial Paraíso samples.

Extended Data Figure 5 | Monthly water balance estimation in the region. a, Comparisons between monthly averaged precipitation (solid dots and triangles) and actual evapotranspiration (AET, open dots and triangles) over Belém and Manaus. The water-balance model[44] as implemented in the USGS Thornthwaite model[45] was used to calculate monthly AET. **b,** As in **a**, but for the LGM conditions. We assume that the cave temperature was ~21^{o}C during the LGM. Rainfall in the region was ~60% of today's as calculated in the Extended Data Table 1, uniformly decreased in each month from today's values. It shows an essentially same pattern as that at present.

Extended Data Figure 6 | Comparisons of the Paraíso record and local insolation curves. The cave $\delta^{18}O$ record spans about 46,000 years, long enough to cover two precessional cycles. However, no obvious correlation can be observed between the cave record with local insolation in month of January (blue), April (cyan), July (dark blue) and October (dark cyan). Insolation data were from ref. 50.

Extended Data Figure 7 | Comparisons of the Paraíso $\delta^{18}O$ and atmospheric greenhouse gas concentrations. Atmospheric CO_2 (blue) and CH_4 (dark blue) concentration changes are recorded in Antarctic ice cores[51,52].

Extended Data Figure 8 | Comparisons of the Paraíso cave record and ice core records. a, Paraíso $\delta^{18}O$ record is compared with the ice core records from Greenland[53] (dark blue, NGRIP Ice Core) and from Antarctica[54] (blue, EDML Ice Core) during the time interval from 25 kyr BP to 45 kyr BP. The NGRIP ice core data are plotted in the AICC12 timescale[55], which is identical to the annual layer-counted GICC05 timescale[56] for the studied time interval. The EDML ice core data are plotted in the AICC12 age scale[55]. The D/O events are marked on the NGRIP record. The strong correlations between the Paraíso record and ice core records confirm the existence of rapid air-sea interactions between the high-latitudes and the tropics on millennial timescales[57,58], likely through the so-called bipolar seesaw mechanism[59]. **b,** As in **a**, but Paraíso Cave record is compared with the ice core records from Greenland[53] (dark blue, NGRIP Ice Core) and from Antarctica[25] (blue, WDC Ice Core). The NGRIP and WDC ice core data are plotted in the WD2014 timescale[25]. The slightly enhanced correlations between the Paraíso record and ice core records, albeit visually, support the chronological method adopted in ref. 60.

Extended Data Figure 9 | Paraíso $\delta^{13}C$ record. Contrary to the stalagmite $\delta^{18}O$ record, Paraíso $\delta^{13}C$ record does not show an obvious shift from the last glacial period to Holocene. In fact, the $\delta^{13}C$ value reaches as low as ~ -10‰ during the LGM, similar to the observed minimum value in Holocene. This suggests that vegetation type in the region has not undergone dramatic change and remains as C3 plant[37,61]. The rainforest in eastern Amazon may have become an open forest when the precipitation significantly decreased during the LGM. However, it was not replaced by savanna or grassland, i.e. not dominated by C4 plants. The $\delta^{13}C$ spikes are likely caused by individual air-water-rock interactions during calcite precipitation.

Extended Data Table 1 | Calculations on water vapor loss amount over the eastern Amazon. a, Cave temperature was assigned 5°C lower in the LGM, and 0.5°C warmer during mid-Holocene, relative to modern values. $\delta^{18}O_c$ is calcite $\delta^{18}O$ value, read from the Paraíso speleothem record. $\delta^{18}O_p$ is local precipitation $\delta^{18}O$ value, calculated using an isotopic fractionation factor between calcite and water derived from the equation: $1000 * \ln \alpha (\text{Calcite-}H_2O) = 17.66 * (10^3 * T^{-1}) – 30.16$, where T is in kelvins[39]. VSMOW: Vienna Standard Mean Ocean Water. $\delta^{18}O_{sw}$ is sea water $\delta^{18}O$, assigned 0‰ for today and mid-Holocene, and 1‰ in the LGM[62,63]. Water vapor fraction remained was calculated using the Rayleigh fractionation equation $(1000 + \delta^{18}O_p) / (1000 + \delta^{18}O_{sw}) = f^{(\alpha - 1)}$, where f is the fraction of the original water vapor remaining in air masses, and α is an isotopic fractionation factor between water liquid and vapor phases[64]. In percentage, water vapor removed from air masses after reaching the cave site is about 36%, 50% and

28% at today, in mid-Holocene, and LGM, respectively. Given a 100% relative humidity, the absolute humidity (AH, g/m^3) can be calculated from equation: $AH = (C * e_s) / T$, where C is a constant with a value of 2,165 gK/J, e_s is saturation vapor pressure in kPa, and T is in kelvin. We obtained the absolute humidity of ~24.3 g/m^3, 25.0 g/m^3 and 18.3 g/m^3 in modern day, mid-Holocene and LGM, respectively. So, the absolute humidity in this equatorial region was about 103% and 75% of today's during the mid-Holocene and LGM, respectively. The amount of moisture removed from air masses is then calculated relative to the modern value. **b,** Same as in **a**, but to test the sensitivity of water vapor loss to temperature, different temperatures were applied for the mid-Holocene (e.g., the same as modern) and LGM (e.g., 4°C or 6°C lower than today's value).

Source Data Tables The data will be available online after publication of the paper.

Table S1 U-Th dating results for Paraíso speleothems

Table S2 $\delta^{18}O$ and $\delta^{13}C$ time series for Paraíso speleothems

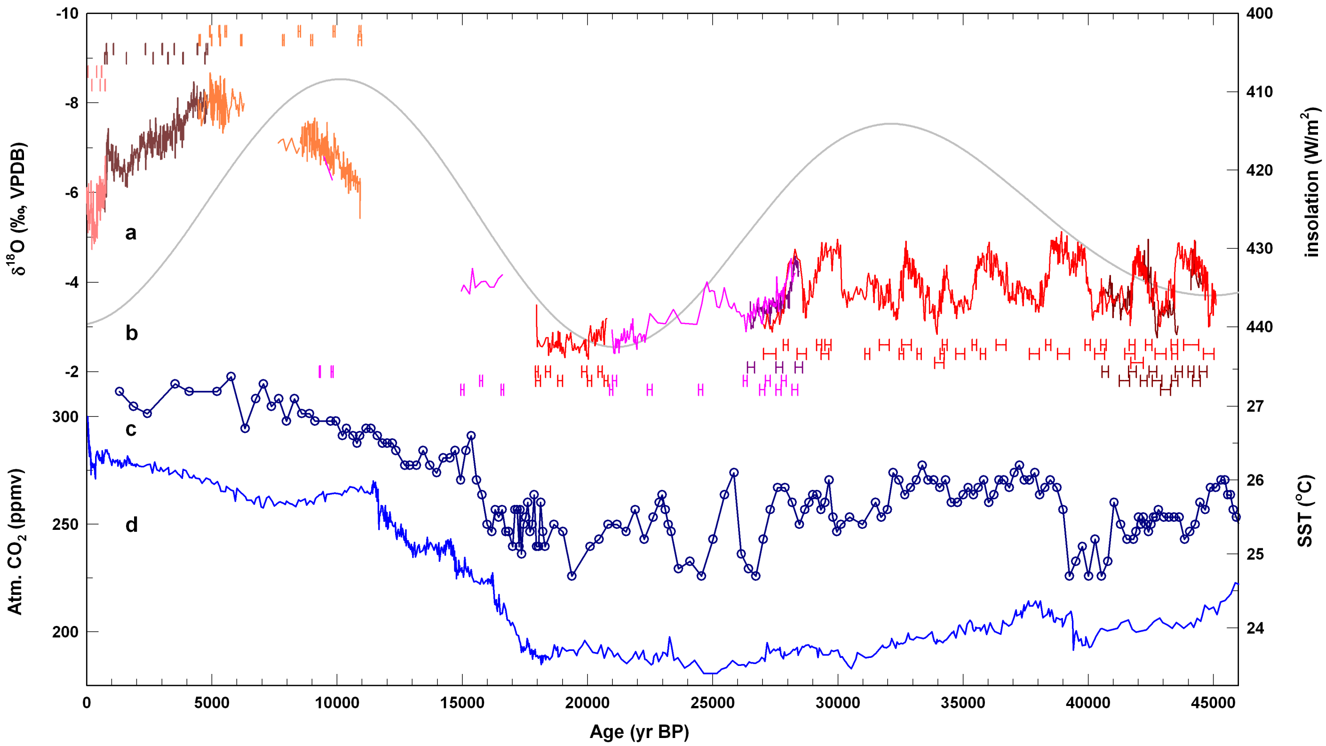

δ¹⁸O (‰, VPDB)
-10
-8
-6
-4
-2
insolation (W/m²)
400
410
420
430
440
27
26
25
24
SST (°C)
Atm. CO₂ (ppmv)
300
250
200
a
b
c
d
0
5000
10000
15000
20000
25000
30000
35000
40000
45000
Age (yr BP)

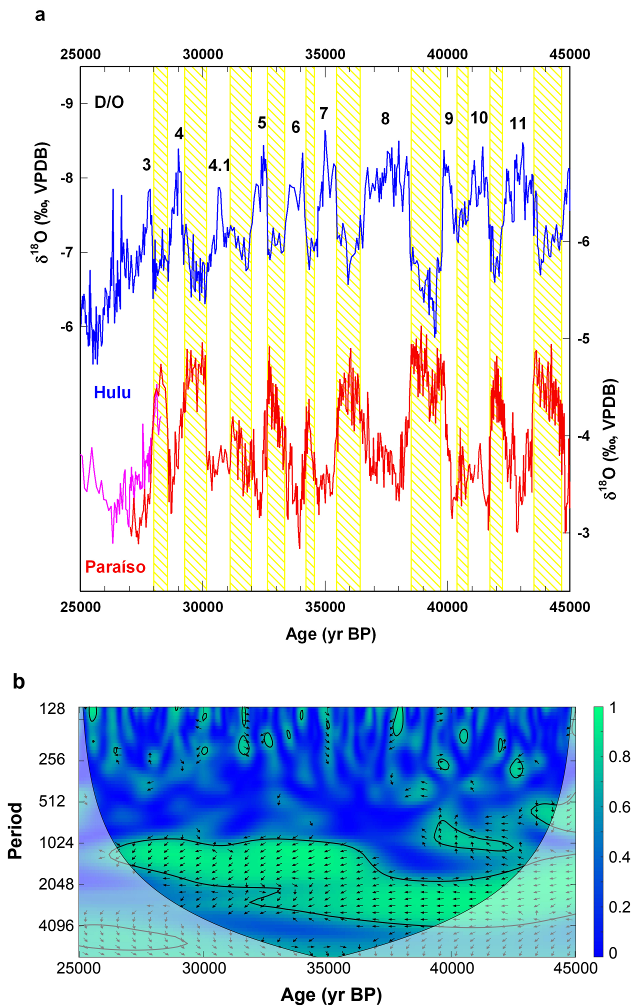

a
25000
30000
35000
40000
45000
D/O
3
4
4.1
5
6
7
8
9
10
11
-9
-8
-7
-6
-6
-5
-4
-3
δ18O (‰, VPDB)
Hulu
Paraíso
Age (yr BP)
b
128
256
512
1024
2048
4096
Period
1
0.8
0.6
0.4
0.2
0
Age (yr BP)

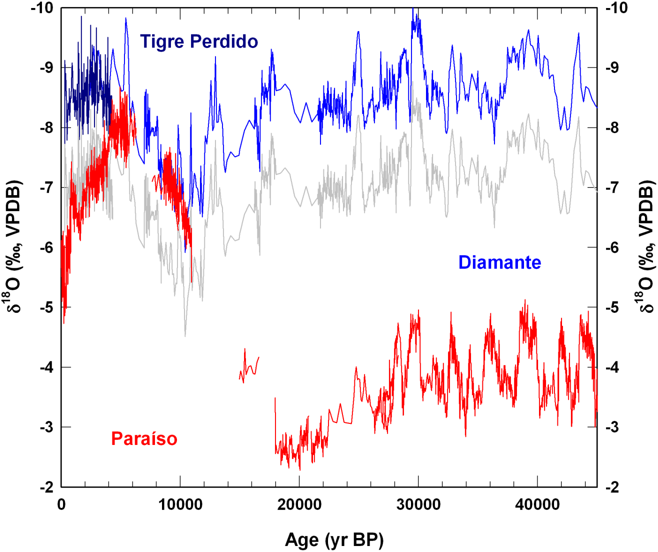

Tigre Perdido
Diamante
Paraíso
δ18O (‰, VPDB)
Age (yr BP)
-10
-9
-8
-7
-6
-5
-4
-3
-2
0
10000
20000
30000
40000